Multibody Syst Dyn
DOI 10.1007/s11044-014-9409-8

Integrated robust controller for vehicle path following

Behrooz Mashadi · Pouyan Ahmadizadeh · Majid Majidi · Mehdi Mahmoodi-Kaleybar

Received: 8 March 2013 / Accepted: 8 January 2014

Abstract The design of an integrated 4WS + DYC control system to guide a vehicle on a desired path is presented. The lateral dynamics of the path follower vehicle is formulated by considering important parameters. To reduce the effect of uncertainties in vehicle parameters, a robust controller is designed based on a μ-synthesis approach. Numerical simulations are performed using a nonlinear vehicle model in MATLAB environment in order to investigate the effectiveness of the designed controller. Results of simulations show that the controller has a profound ability to making the vehicle track the desired path in the presence of uncertainties.

Keywords Vehicle path following · 4WS · DYC · Robust control · μ-Synthesis

Notation

Alphabetic

A	State-space matrix
B	Input matrix
C	Output matrix
$\mathbb{C}$	Set of complex numbers
$C_{\alpha f}$ ($C_{\alpha r}$)	Cornering stiffness of front (rear) tires
d	Output from perturbation block
D	Constant scaling matrix
E	Disturbance matrix
c.g.	Center of gravity

B. Mashadi · P. Ahmadizadeh (✉) · M. Majidi
School of Automotive Engineering, Iran University of Science and Technology, Tehran, Iran
e-mail: p_ahmadizadeh@iust.ac.ir

M. Majidi
e-mail: m_majidi@iust.ac.ir

M. Mahmoodi-Kaleybar
School of Mechanical Engineering, Iran University of Science and Technology, Tehran, Iran
e-mail: m_mahmoodi_k@iust.ac.ir

Published online: 05 February 2014

e_u	Weighted control input
e_z	Output weighted signal
F_{yf} (F_{yr})	Lateral force of front (rear) tires
F_u	Upper LFT
G_{sys}	System nominal model
i	Scaled disturbance input
I_z	Vehicle moment of inertia around z axis
inf	Infimum
L_f (L_r)	Distance from vehicle center of gravity to front (rear) axle
LFT	Linear fractional transformation
m	Vehicle mass
M_z	External yaw moment produced by DYC system
U	Controller input
p ($\bar{p}$)	Uncertain (nominal) parameter
Q	Parameter nominal dispersion
r ($\dot{r}$)	Lateral position (velocity) error
$\dot{R}$ ($\dot{R}_d$)	Vehicle real (desired) velocity
$\Re$	Set of real numbers
S	Sensitivity function
sup	Supremum
u	Vehicle longitudinal velocity
u_d	Desired longitudinal velocity
v	Vehicle lateral velocity
v_d	Desired lateral velocity
V	Vehicle velocity
w	Input to perturbation block
W	Disturbance vector
W_z, W_u, W_ρ	System output, control input, road input weighting functions
x, y, z	Coordinate system attached to the vehicle
X	State-space vector
Z	Output signal

Greek

α_f (α_r)	Side slip angle of front (rear) tires
β_f (β_r)	Angle of front (rear) tire velocity with longitudinal axis of vehicle
δ	Perturbation
δ_f (δ_r)	Front (rear) steering angle
Δ_F	Fictitious uncertainty block
Δ_{sys}	Uncertain matrix
ρ	Radius of curvature of the desired path
μ	Structured singular value
$\bar{\sigma}$	Maximum singular value
ω	Frequency
ψ ($\dot{\psi}$)	Yaw angle (rate)
ψ_d ($\dot{\psi}_d$)	Desired yaw angle (rate)
ψ_e	Orientation error

1 Introduction

With the population growth, the numbers of vehicles and passengers have been increased in the streets and highways leading to more traffic problems. Several measures such as building new highways and roads have been considered in order to reduce traffic congestion and increasing safety, but such measures do not always suffice because of environmental and cost constraints. One way to improve the safety of roads is to remove the human element errors during driving. This can lead to automatic driving technology, which is the fundamental of intelligent transportation systems (ITS) and is being studied by many researchers during recent years. The primary task of automatic driving is to make an autonomous vehicle to follow a reference path automatically. During this path following, therefore, several issues should be considered to have an acceptable path control. Vehicle controllers that meet these requirements are called path followers.

The goal of a path-following controller is to minimize the lateral distance between the vehicle and a defined path, to minimize the difference in the vehicle and the path headings and to limit the control input to smoothen the motions while maintaining the stability. Several studies have been carried out regarding the path-following problem. El Hajjaji et al. [1] focused on the design of a stabilizing fuzzy controller for the path-following problem of vehicles using a nonlinear dynamics model. The vehicle model is approximated by a set of linear models interpolated by fuzzy membership functions, and then a model-based fuzzy controller is developed to stabilize the model. Then the outcome of the path-following problem is parameterized in terms of a linear matrix inequality (LMI) problem. The LMI problem is solved by a convex optimization technique to complete the fuzzy path-following control design for vehicles. Consolini et al. [2] considered a special path-following task so that a given front point of a car-like vehicle, which is within the look-ahead range of a stereo vision system, to follow a prespecified Cartesian path. A solution to this path-following problem was provided by a feedback/feedforward control strategy where the feedforward was determined by a dynamic generator based on exact dynamic inversion over the nominal vehicle model and the feedback was mainly issued by correcting terms proportional to the tangential and normal errors determined with respect to the vehicle's ideal trajectory. Balluchi et al. [3] considered a kinematic model of a nonholonomic wheeled vehicle to follow a path. They assumed that the current distance and the heading angle error with respect to the closest point on the reference path can be measured but only the sign of the path curvature is detected. They used a hybrid system formalism to model the problem based on optimal control theory, as the feedback information was both continuous and discrete. Hellström et al. [4] propose a path-tracking algorithm called Follow the Past, in which a human driver drives the path once, while the computer records the position, velocity, orientation, and steering angle. Then this piece of information is used to control the vehicle each time it autonomously travels along the path. If the vehicle gets off the course, for example, as a result of avoiding an obstacle or because of noise in positioning sensors, the Follow the Past algorithm steers like the driver, plus an additional angle, based on the distance to the path. Heredia et al. [5] present a method to analyze the stability of an autonomous vehicle path-following algorithm taking into account explicitly the computation and communication delays in the control loop. These pure delays are present in autonomous vehicles due to position estimation. The problem is analyzed by solving directly the transcendental characteristic equation that appears when the time delay is considered. The analysis is carried out for straight paths and paths of constant curvature, and the method is applied to the pure pursuit path-tracking algorithm. Goodarzi et al. [6] treated this problem by the application of a linear quadratic regulator (LQR) technique. They used an integrated controller comprising

an active front steering (AFS) in low lateral acceleration regimes and a direct yaw moment control (DYC) system for high-g maneuvers. The road curvature and the lateral offset between the desired path and the vehicle were taken as the feedback/feed-forward signals that produce both the front steering angle and the external yaw moment signals as the control efforts.

With the developments of robust control theories, applications of robust controllers have become feasible. One important application of robust control is in vehicles, namely in aerial, maritime, and ground vehicles. Examples are a robust controller for altitude tracking and stability augmentation of an unmanned autonomous air vehicle [7] and control of an autonomous underwater vehicle using H_∞ control [8]. Several works are also devoted to ground vehicles. Hiraoka et al. [9] propose an automatic path-tracking controller of a four-wheel steering vehicle based on the sliding-mode control theory. The front and rear wheel steerings are decoupled at front and rear control points and are defined as centers of percussion with respect to the front and rear wheels, respectively. The front/rear control points are then regulated by the front/rear steering to make a good tracking of the desired path. In [10] Moriwaki proposes an autonomous steering controller for path following using nonlinear state feedback H_∞ control, and the deviation of the vehicle from the planned path, which is calculated from the data of a CCD camera, is kept small by feedback control via the steering motors. Ackermann et al. [11] consider designing linear and nonlinear controllers for automatic steering of a city bus using sliding mode control.

DYC, 4WS, and their combinations as well as the robust control systems have been extensively used for vehicle dynamics control purposes. The current paper makes advantage of both DYC + 4WS vehicle dynamics methods together with a robust control methodology in order to design a new path-following system for autonomous ground vehicles. The controller is designed based on the μ-synthesis method incorporating 4WS and DYC systems. The aim is to design an advanced controller with large number of control inputs in order to improve the path-following problem and at the same time to account for the structured uncertainties.

The paper is organized as follows. Section 2 is devoted to vehicle dynamics modeling and formulation based on the path-following considerations. Section 3 deals with the design of controllers suitable for path following aims. The robust performance and the robust stability analysis of the controller in the μ-framework are also discussed in this section. The performance of the controller is examined in Section 4 based on a simulation analysis with a nonlinear vehicle model. Finally, the work is concluded in Section 5.

2 Modeling

Mathematical modeling of vehicle motion is necessary for both control and simulation purposes. The former will be discussed in the following subsections, whereas the simulation program is based on a previous published work.

2.1 The single track model

A single-track vehicle model with two degrees of freedom, comprising the lateral position y and yaw angle ψ, is shown in Fig. 1. The lateral position is measured along the lateral axis of the vehicle toward the center of rotation of the vehicle, and the vehicle yaw angle ψ is measured with respect to the global axis X. This single-track model has three inputs: the front steering angle δ_f, the rear steering angle δ_r, and the external yaw moment M_z around the z axis of the vehicle.

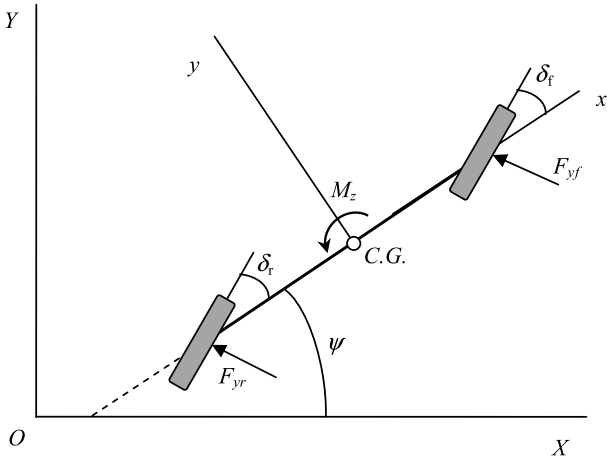

Fig. 1 The single-track model

The dynamic translational and rotational equations of the single-track model read [12]

$$m(\dot{v} + u\dot{\psi}) = F_{yf} + F_{yr}, \tag{1}$$

$$I_z\ddot{\psi} = L_f F_{yf} - L_r F_{yr} + M_z, \tag{2}$$

where F_{yf} and F_{yr} are tire lateral forces at front and rear, respectively, and u is the vehicle longitudinal speed. L_f and L_r are the distances of front and rear axles from the c.g. of the vehicle. m and I_z are the vehicle mass and its mass moment of inertia around the z axis, respectively. The tire lateral forces are defined as

$$F_{yf} = 2C_{\alpha f}\left(\delta_f - \frac{v + L_f\dot{\psi}}{u}\right), \tag{3}$$

$$F_{yr} = 2C_{\alpha r}\left(\delta_r - \frac{v - L_r\dot{\psi}}{u}\right), \tag{4}$$

where $C_{\alpha f}$ and $C_{\alpha r}$ are front and rear cornering stiffness. The factor 2 is to account for the two tires on each axle. Substituting Eqs. (3) and (4) into Eqs. (1) and (2), the translational and rotational equations of the single-track model can be obtained as

$$\dot{v} = \left(-\frac{2C_{\alpha f} + 2C_{\alpha r}}{mu}\right)v + \left(-u - \frac{2C_{\alpha f}L_f - 2C_{\alpha r}L_r}{mu}\right)\dot{\psi} + \left(\frac{2C_{\alpha f}}{m}\right)\delta_f + \left(\frac{2C_{\alpha r}}{m}\right)\delta_r, \tag{5}$$

$$\ddot{\psi} = \left(-\frac{2L_fC_{\alpha f} - 2L_rC_{\alpha r}}{I_z u}\right)v + \left(-\frac{2L_f^2C_{\alpha f} + 2L_r^2C_{\alpha r}}{I_z u}\right)\dot{\psi} + \left(\frac{2L_fC_{\alpha f}}{I_z}\right)\delta_f + \left(-\frac{2L_rC_{\alpha r}}{I_z}\right)\delta_r + \left(\frac{1}{I_z}\right)M_z. \tag{6}$$

2.2 Path-following problem

In this section, a dynamic path-following model is derived based on the single-track model and with the state variables in terms of position and orientation error. The configurations of the actual and desired vehicle orientations are demonstrated in Fig. 2. The xy frame

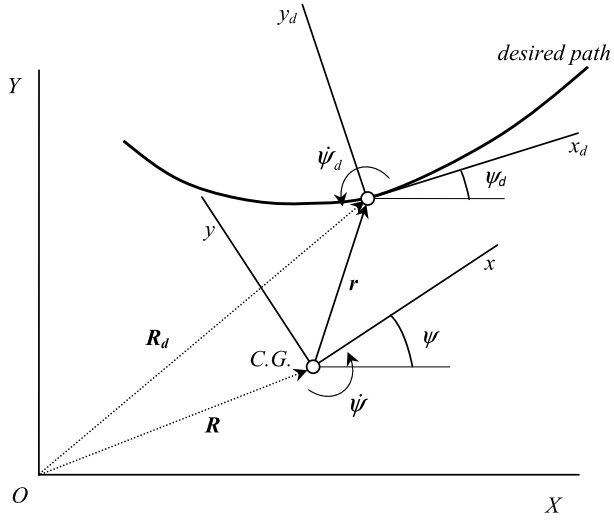

Fig. 2 The path-following configuration

represents the vehicle orientation on its actual path, whereas the $x_d y_d$ frame represents the vehicle orientation on its desired path. The goal is to minimize both the lateral position and orientation errors relative to the desired path, in order to provide a desired path control.

The orientation error and its derivative can be written as [13]

$$\psi_e = \psi - \psi_d, \tag{7}$$

$$\dot{\psi}_e = \dot{\psi} - \dot{\psi}_d, \tag{8}$$

where $\dot{\psi}_d$ is the rate of change of the desired orientation of the vehicle and is defined as

$$\dot{\psi}_d = \frac{u}{\rho}, \tag{9}$$

where ρ is the radius of curvature of the desired path. The lateral position error vector $\mathbf{r}$ can be defined in the mobile frame x–y as

$$\mathbf{r} = x_e \hat{i} + y_e \hat{j}, \tag{10}$$

where the derivative of y_e can be obtained as

$$\dot{y}_e = v + u\psi_e. \tag{11}$$

Substituting Eqs. (7) and (11) and their derivatives into Eqs. (5) and (6) yields the state space form of the dynamic path-following problem:

$$\begin{aligned} \dot{X} &= [A]X + [B]U + [E]W \\ Z &= [C]X + \left[D^B\right]U + \left[D^E\right]W, \end{aligned} \tag{12}$$

where the matrices A, B, E, C, D^B, D^E and the state, input, and disturbance vectors X, U, and W are:

$$A = \begin{bmatrix} 0 & 1 & 0 & 0 \\ 0 & -2\frac{C_{\alpha f}+C_{\alpha r}}{mu} & 2\frac{C_{\alpha f}+C_{\alpha r}}{m} & 2\frac{-C_{\alpha f}L_f+C_{\alpha r}L_r}{mu} \\ 0 & 0 & 0 & 1 \\ 0 & 2\frac{-C_{\alpha f}L_f+C_{\alpha r}L_r}{I_z u} & 2\frac{C_{\alpha f}L_f-C_{\alpha r}L_r}{I_z} & -2\frac{C_{\alpha f}L_f^2+C_{\alpha r}L_r^2}{I_z u} \end{bmatrix}, \tag{13}$$

$$B = \begin{bmatrix} 0 & 0 & 0 \\ \frac{2C_{\alpha f}}{m} & \frac{2C_{\alpha r}}{m} & 0 \\ 0 & 0 & 0 \\ \frac{2C_{\alpha f}L_f}{I_z} & -\frac{2C_{\alpha r}L_r}{I_z} & \frac{1}{I_z} \end{bmatrix}, \qquad E = \begin{bmatrix} 0 \\ 2\frac{-C_{\alpha f}L_f + C_{\alpha r}L_r}{m} - u^2 \\ 0 \\ -2\frac{C_{\alpha f}L_f^2 + C_{\alpha r}L_r^2}{I_z} \end{bmatrix}, \tag{14}$$

$$C = \begin{bmatrix} 1 & 0 & 0 & 0 \\ 0 & 0 & 1 & 0 \end{bmatrix}, \qquad D^E = [0]_{2\times 1}, \qquad D^B = [0]_{2\times 3},$$

$$X = \begin{Bmatrix} y_e \\ \dot{y}_e \\ \psi_e \\ \dot{\psi}_e \end{Bmatrix}, \qquad U = \begin{Bmatrix} \delta_f \\ \delta_r \\ M_z \end{Bmatrix}, \qquad W = \left\{\frac{1}{\rho}\right\}. \tag{15}$$

Equation (12) serves as the form that will be used to define the uncertain state space model. In this equation, A is the state matrix, B is the input matrix, E is the disturbance matrix, C is the output matrix, and D^E and D^B are feedthrough matrices corresponding to the disturbance and control inputs, respectively. It should be noted that Z consists of the lateral distance error (y_e) and the orientation error (ψ_e) described earlier.

3 Controller design

In this section, the design process for the proposed controller is discussed. The intention is to design a robust controller for the vehicle path-following problem in the presence of uncertainties. This control method lets one to consider unstructured and parametric uncertainties due to un-modeled dynamics, simplifications, neglected nonlinearities, and system parameter variations. This is something that is impossible or is with great difficulty to include in other control methods.

3.1 Uncertainties

The dynamic path-following state space model described by Eq. (12) contains uncertainties due to the variations of parameters around their nominal values. Based on the road conditions, the characteristics of tire and road vary, and as a result the tire-road friction coefficient also varies. The influence of friction coefficient variations can be considered in the cornering stiffnesses $C_{\alpha f}$ and $C_{\alpha r}$.

Considering p as an uncertain parameter of the vehicle, it can be expressed as the sum of two nominal and uncertain parts written in the form of a multiplicative perturbation [14]:

$$p = \bar{p}(1 + Q\delta), \tag{16}$$

where $\bar{p}$ is the nominal value, Q is the nominal dispersion of the parameter and considered to vary between 5 % and 45 %, and δ is an unknown perturbation satisfying $\|\delta\| \leq 1$. According to Eq. (16), the cornering stiffness can be described as

$$C_{\alpha f} = \bar{C}_{\alpha f}(1 + Q_f\delta_1), \tag{17}$$

$$C_{\alpha r} = \bar{C}_{\alpha r}(1 + Q_r\delta_2). \tag{18}$$

Equations (17) and (18) are used to define uncertain form of the front and rear cornering stiffness. Including the uncertainties due to the cornering stiffness makes the state space

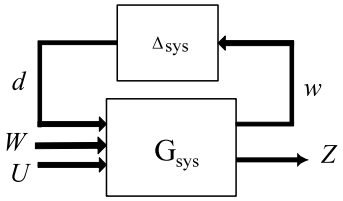

Fig. 3 The upper LFT description

model of the vehicle uncertain. Therefore, the uncertain path-following state space model replacing Eq. (12) is

$$G(s) = \begin{bmatrix} A_0 & E_0 & B_0 \\ C_0 & D_0^E & D_0^B \end{bmatrix} + \sum_{i=1}^{2} \delta_i \begin{bmatrix} A_i & E_i & B_i \\ C_i & D_i^E & D_i^B \end{bmatrix}. \tag{19}$$

Using the vehicle data given in Table 3 (Appendix A), the matrices in Eq. (19) are evaluated and provided in Appendix B.

In order to construct the model suitable for a robust controller design, the uncertain state space model must be described in a Linear Fractional Transformation (LFT) form. The LFT structure can be constructed using Singular Value Decomposition (SVD) method by which the uncertainty matrix can be decomposed into [14]

$$\begin{bmatrix} A_i & E_i & B_i \\ C_i & D_i^E & D_i^B \end{bmatrix} = \begin{bmatrix} P_i \\ V_i \end{bmatrix} \begin{bmatrix} S_i & T_i & J_i \end{bmatrix}, \tag{20}$$

where P_i and V_i are variables used to relate the system state derivatives and outputs to the output of uncertainty matrix. S_i, T_i, and J_i are used to define uncertainty matrix inputs in the LFT form. Using decomposed matrices, the perturbed equations can be obtained as

$$\begin{bmatrix} \dot{x} \\ w_1 \\ w_2 \\ Z \end{bmatrix} = \begin{bmatrix} A_0 & P_1 & P_2 & E_0 & B_0 \\ S_1 & 0 & 0 & T_1 & J_1 \\ S_2 & 0 & 0 & T_2 & J_2 \\ C_0 & V_1 & V_2 & D_0^E & D_0^B \end{bmatrix} \begin{bmatrix} x \\ d_1 \\ d_2 \\ W \\ U \end{bmatrix} = \left[G_{\text{sys}}(s) \right] \begin{bmatrix} x \\ d_1 \\ d_2 \\ W \\ U \end{bmatrix}, \tag{21}$$

where G_{sys} is the interconnection matrix. Figure 3 represents the upper LFT description in which w is the input vector to the perturbation block and d is its output vector, whereas Z represents the output signals to be minimized and includes both performance and robustness measures. The perturbation block Δ_{sys} corresponds to parameter variations and is a diagonal matrix. W and U denote the disturbance and controller inputs, respectively. The disturbance is the input from road curvature, and the controller inputs include vehicle's front steering angle (δ_f), the rear steering angle (δ_r), and the external yaw moment (M_z).

Considering the state space model and decomposed matrices, the interconnection matrix G_{sys} is evaluated for the vehicle data and presented in Appendix B.

Therefore, the input/output relation of the perturbed model is described by the upper LFT as

$$Z = F_u(G_{\text{sys}}, \Delta_{\text{sys}}) \begin{bmatrix} W \\ U \end{bmatrix} \tag{22}$$

with the diagonal, uncertain matrix

$$\Delta_{\text{sys}} = \begin{bmatrix} \delta_1 & 0 \\ 0 & \delta_2 \end{bmatrix}. \tag{23}$$

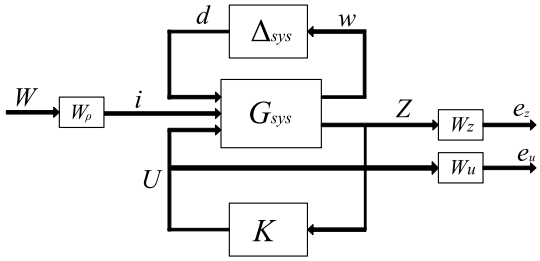

Fig. 4 Interconnection structure of the closed-loop system

3.2 Design specifications

The block diagram of the closed-loop system, which includes the vehicle model, the feedback structure, and the controller, as well as the elements reflecting the model uncertainties and the performance objectives, is depicted in Fig. 4, where i is the scaled disturbance input from the road. The closed-loop system output e_z may be determined by

$$e_z = \mathbf{S}W, \tag{24}$$

where the matrix $\mathbf{S} = \mathbf{S}(G_{\text{sys}})$ is considered as the nominal sensitivity function with respect to the input W from the road. The performance objective requires the transfer function from W to e_z and e_u (defined as $e_u = \mathbf{KS}W$) to be small in the sense of $\|.\|_\infty$ for all possible (stable) uncertainty matrices Δ_{sys}. The transfer function matrices W_z and W_u of Fig. 4 are used to reflect the relative significance over different frequency ranges for which the performance is required. In this work, the performance weighting function is a scalar function and is chosen in such a way that to ensure, apart from good disturbance attenuation, a good transient response. The numerical result is

$$W_z = \begin{bmatrix} 1.7\frac{s^2+1.8s+10}{s^2+4s+0.01} & 0 \\ 0 & 0.005\frac{s^2+1.8s+10}{s^2+8s+0.01} \end{bmatrix}. \tag{25}$$

Figure 5 illustrates the variation of weighting functions with frequency. It is clear that at low frequencies the effect of the steady-state output for W_{z1} and W_{z2} is in order of 5×10^{-3} and 0.2 (or less), respectively. This performance requirement becomes less stringent with increasing frequency so that the disturbance is no longer influential from above 10 rad/s frequency. The control weighting function W_u is chosen based on the input physical limitations. To limit control input deflections, weighting functions W_{ul} and W_{u2} are obtained by considering maximum steering angles of 35 and 20 degrees for the front and rear wheels, respectively; W_{u3} is considered to limit the maximum corrective external yaw moment to 5000 N m. W_ρ is used to scale the disturbance from the road, considering the minimum radius of 100 m that a vehicle can follow at high-g maneuvers [14]. Numerical values for these factors are given in Table 1.

The design problem for the vehicle system is to find a linear controller $K(s)$ to generate the output feedback $U(s) = K(s)Z(s)$, to ensure the following properties of the closed-loop system.

3.2.1 Nominal performance

The closed-loop system achieves nominal performance if the following performance objective is satisfied for the nominal plant model G_{sys}:

$$\left\| \begin{matrix} W_\rho W_z S(G_{\text{sys}}) \\ W_\rho W_u K S(G_{\text{sys}}) \end{matrix} \right\|_\infty < 1, \tag{26}$$

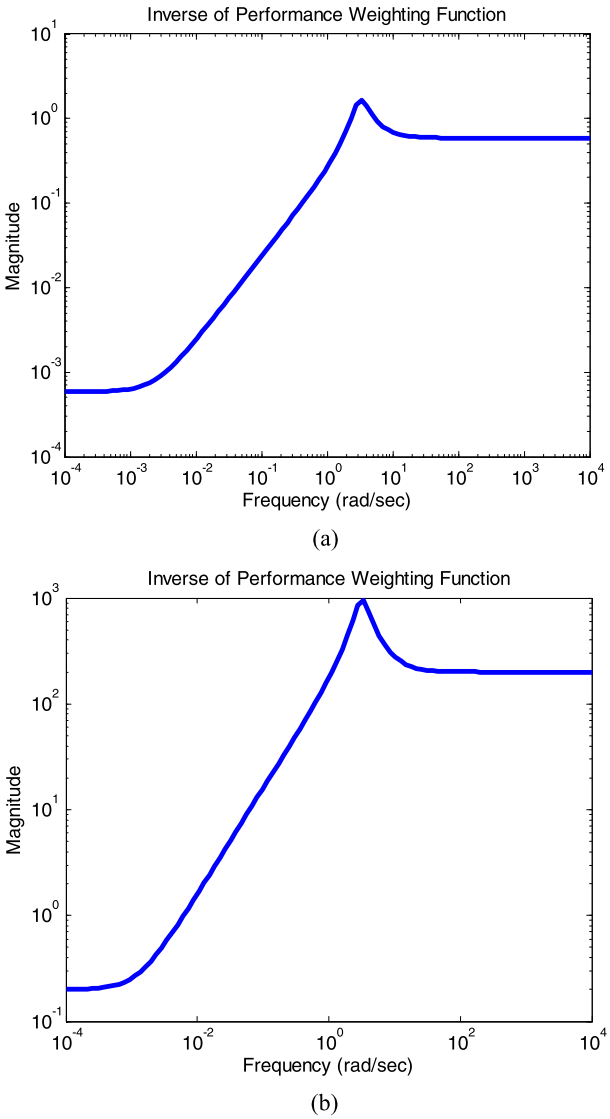

Fig. 5 (**a**) Singular values of $\frac{1}{W_{z1}}$ (**b**) Singular values of $\frac{1}{W_{z2}}$

Table 1 Weighting factors

Factor	Value
W_{ul}	1.637
W_{u2}	2.865
W_{u3}	2×10^{-4}
W_{ρ}	0.010

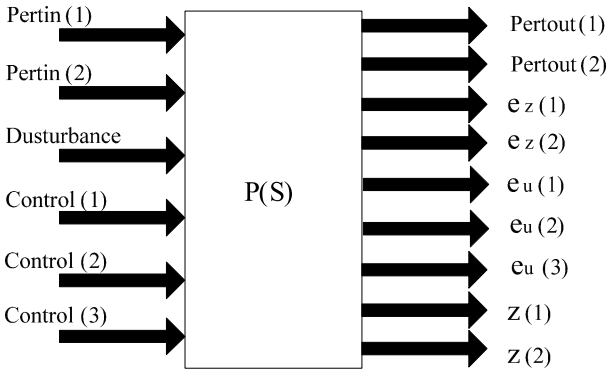

Fig. 6 Schematic diagram of the open-loop system

where W_ρ, W_z, and W_u are appropriately chosen weighting functions. This objective corresponds to the mixed S/KS sensitivity optimization [14].

3.2.2 Robust stability

The closed-loop system achieves robust stability if the closed-loop system is internally stable for each possible, perturbed plant dynamics $G = F_u(G_{\text{sys}}, \Delta_{\text{sys}})$ [14].

3.2.3 Robust performance

The closed-loop system must maintain, for each $G = F_u(G_{\text{sys}}, \Delta_{\text{sys}})$, the performance objective [14]

$$\left\| \begin{matrix} W_\rho W_z S(G) \\ W_\rho W_u K S(G) \end{matrix} \right\|_\infty < 1. \tag{27}$$

3.3 μ-Synthesis controller design

Let $P(s)$ denote the transfer function matrix of the six inputs–nine outputs open-loop system in Fig. 6, and let the block structure Δ_p be defined for the case of robust performance analysis as

$$\Delta_P := \left\{ \begin{bmatrix} \Delta_{\text{sys}} & 0 \\ 0 & \Delta_F \end{bmatrix} : \Delta_{\text{sys}} \in \Re^{2\times 2}, \Delta_F \in \mathbb{C}^{1\times 5} \right\}, \tag{28}$$

in which $\Re$ and C are the sets of real and complex numbers.

The first uncertainty block Δ_{sys} of this structured matrix is diagonal and corresponds to the uncertainties used in the modeling of the vehicle system. The second block Δ_F is a fictitious uncertainty block that is introduced to represent the performance requirements in the frame of the μ-approach.

To meet the design objectives, a stabilizing controller $K(s)$ is to be found such that, at each frequency $\omega \in [0, \infty]$, the structured singular value μ satisfies the condition

$$\mu_{\Delta_P}\left[F_l(P, K)(j\omega)\right] < 1. \tag{29}$$

The fulfillment of this condition guaranties robust performance of the closed-loop system as in (27). An iterative method called D-K iteration μ-synthesis method is proposed in [15]

Table 2 Controller characteristics

Characteristic	Upper bound margin	Lower bound margin
Robust stability	2.2222	2.1147
Robust performance	1.0743	1.0743

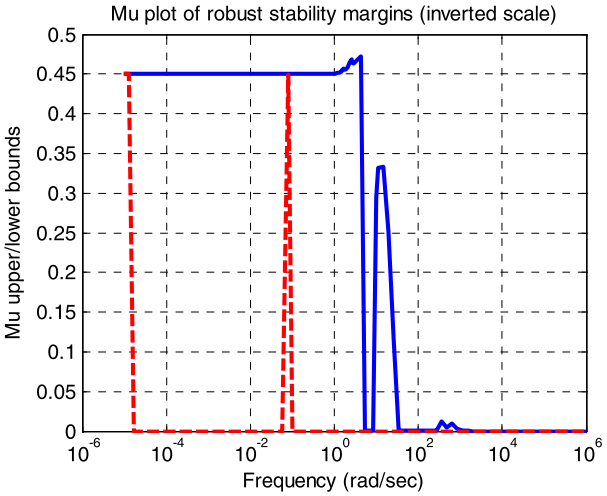

Fig. 7 μ-Plot of robust stability margins

to solve Eq. (29). It is based on solving the following problem for a stabilizing controller K and a diagonal constant scaling matrix D:

$$\inf_{K(s)} \sup_{\omega\in\Re} \inf_{D\in\mathbf{D}} \bar{\sigma}\left[DF_l(P,K)D^{-1}(j\omega)\right]. \tag{30}$$

The controller for the vehicle path-following is designed based on the above procedure within MATLAB environment. To this end, uncertain parameters are defined, and their uncertainty domains are determined based on the physical characteristics of the parameters. Then, the uncertain model of the path-following system is defined as well as determining weighting functions. Next, the configuration of the control system is constructed considering Fig. 4, and finally, the μ-synthesis controller is designed based on the D-K iteration method for the open-loop interconnection. In Table 2 the robust characteristics of the designed controller are demonstrated. The robust stability margin and robust performance margin are two important characteristics of a robust controller, which are also shown in Figs. 7 and 8.

The robust stability margin is the size of the smallest deviation from nominal of the uncertain elements that leads to system instability and is shown in Fig. 7. A robust stability margin greater than 1 means that the uncertain system is stable for all values of its modeled uncertainty. Considering Table 2 and Fig. 7, it is determined that the uncertain system is robustly stable and can tolerate up to 211 % of the modeled uncertainty.

Due to the presence of specific values of uncertain elements, the performance of a nominally stable uncertain system model will degrade. Figure 8 indicates the robust performance margin, which is a measure of the level of degradation brought on by the modeled uncertainty. Figure 8 shows that in the upper bound of the modeled uncertainty, the performance gain of plant with controller is always smaller than unity, which always satisfies Eq. (27). It should be mentioned that in Figs. 7 and 8, the exact robust stability and robust performance margin lies between upper and lower bounds.

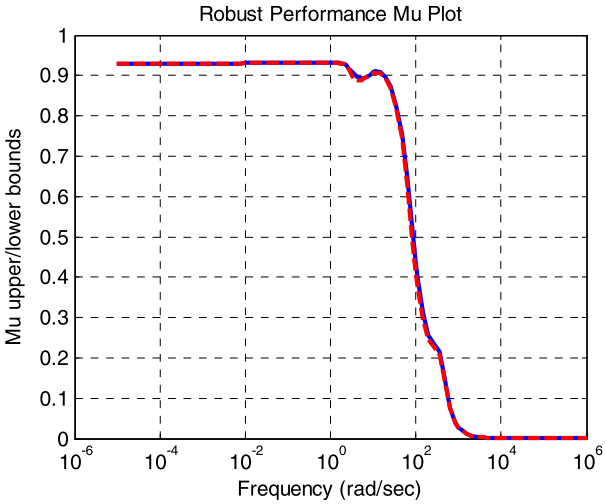

Fig. 8 μ-Plot of robust performance margins

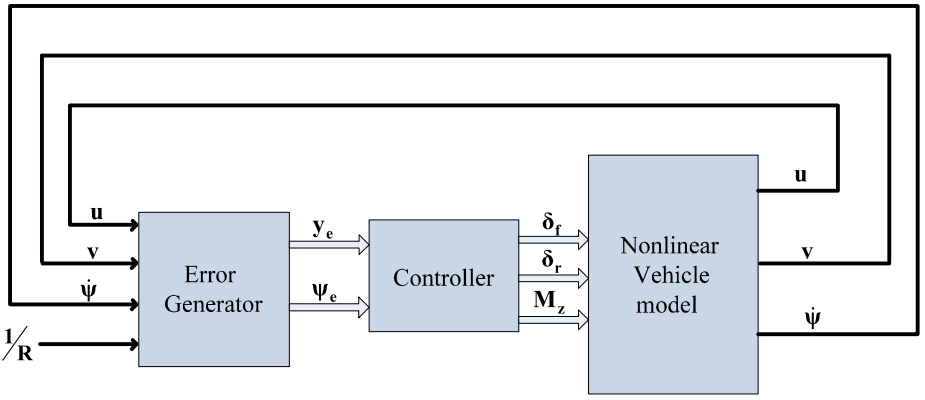

Fig. 9 Configuration of the simulation

4 Numerical simulations

In this section, numerical simulations are carried out to evaluate the performance of the designed controller. An eight-degrees-of-freedom nonlinear vehicle model is used to simulate the behavior of the real vehicle. This simulation is used in several previous work of the author (e.g., [16]). Figure 9 demonstrates the simulation configuration built in the environment of MATLAB software [17].

The robust controller generates the required commands for the vehicle in a given maneuver *with a known constant speed* based on the lateral distance and orientation errors that are calculated by using feedbacks from the vehicle response and road feedforward. The external M_z torque is applied to the vehicle through applying brake to one of the wheels. The braking wheel selection is as follows:

- Turning left ($r > 0$)
  - $M_z > 0$: Brake on rear left wheel
  - $M_z < 0$: Brake on front right wheel

- Turning right ($r < 0$)
  - $M_z > 0$: Brake on front left wheel
  - $M_z < 0$: Brake on rear right wheel

The braking force of the corresponding tire produces a yaw moment M_z around the vehicle center of gravity. The effect of longitudinal slip on the lateral force is taken into account by using the combined slip Pacejka tire model [18].

Two maneuvers are considered to investigate the performance of the controller: (a) A constant radius circular path; (b) A lane change maneuver during which the vehicle moves in a path with two different radii.

Also, in order to make the performance of the controller comparable, each maneuver is also performed by three other controllers namely AFS, 4WS, and AFS + DYC described below:

- The AFS controller has only the front steering angle for input
- The 4WS controller with both the front and rear steering angle inputs
- The AFS + DYC controller has the front steering angle and the external yaw moment as two control inputs

It should be mentioned that the structure of all controllers are similar and the process of designing the controllers is the same as that of the 4WS + DYC controller.

4.1 Circular path

In this maneuver the vehicle with a constant speed of 30 m/s suddenly enters a circular path of 120 meters radius with the road friction coefficient of 0.9. Simulation results are shown in Fig. 10.

Figure 10a shows the lateral distance error of the vehicle for all controllers. As it can be seen the magnitude of this error for the 4WS + DYC controller is lower than those of the other controllers. The same trend is observed from Fig. 10b for the orientation error of the vehicle. Although the performances of the 4WS and AFS + DYC controllers are close in Fig. 10a, but the 4WS controller shows better efficacy in Fig. 10b. This shows the usefulness of the steerability of the rear wheels in 4WS systems in reducing the side slip angle of the vehicle and hence reduction in the orientation error.

Figures 10c and 10d show the variation of the front and rear steering angles of the vehicle, respectively. The steering angles of those systems with the DYC controller are larger than those of the other controllers. The reason is that the steering ability is enhanced due to the yaw moments that are applied by the act of DYC system presented in Fig. 10e. In fact, the yaw moment produced by the DYC system provides grounds for increase of tire slip angles and in turn the tire lateral forces. The 4WS + DYC system benefits from this effect both in the front and rear. Proper adjustments of steer angles in the front and rear makes it possible to adjust the total lateral force acting on the vehicle and at the same time produce the necessary yaw moment for the turning of the vehicle. This is why the 4WS + DYC system has a better response compared to the other systems.

The orientation error, as seen from Fig. 10b, does not die out in a circular maneuver and thus results in a steady-state error. This is a natural result of the vehicle dynamics equations, and in order to observe it, the side slip angle of the vehicle can be written as

$$\beta = \frac{v}{u} = \frac{1}{u}(\dot{y}_e - u\psi_e). \tag{31}$$

Fig. 10 Simulation results of the circular maneuver

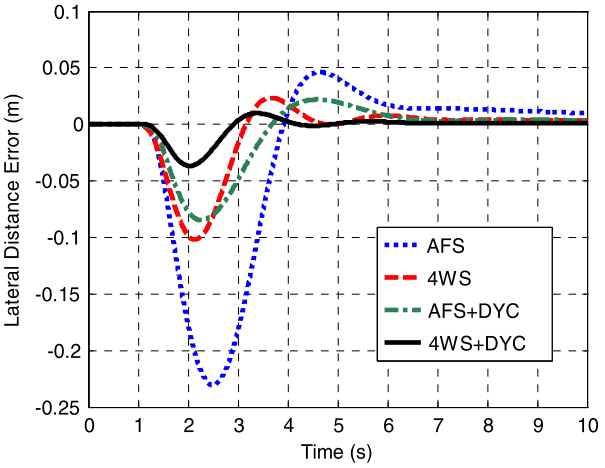

(a) Lateral Distance Error

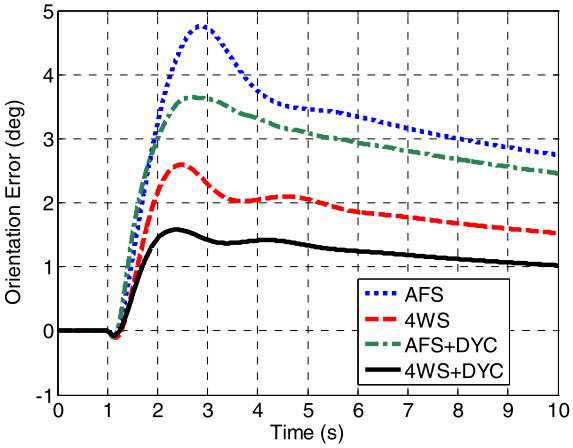

(b) Orientation Error

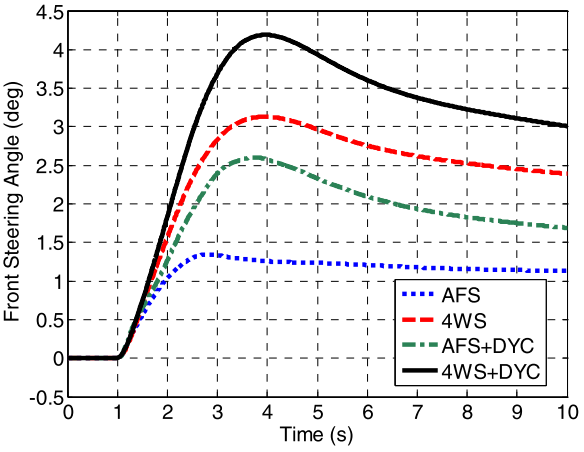

(c) Front Steering Angle

Fig. 10 (*Continued*)

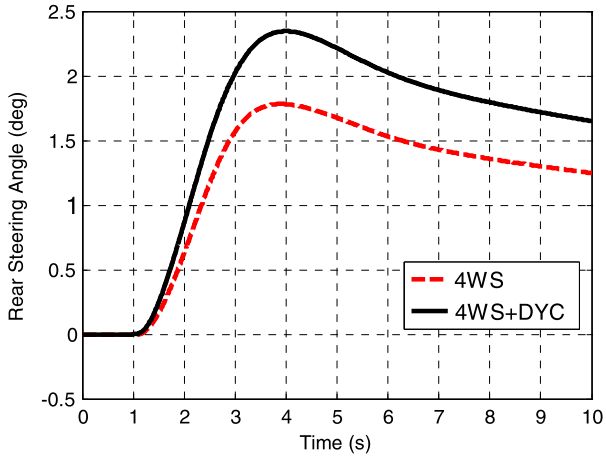

(d) Rear Steering Angle

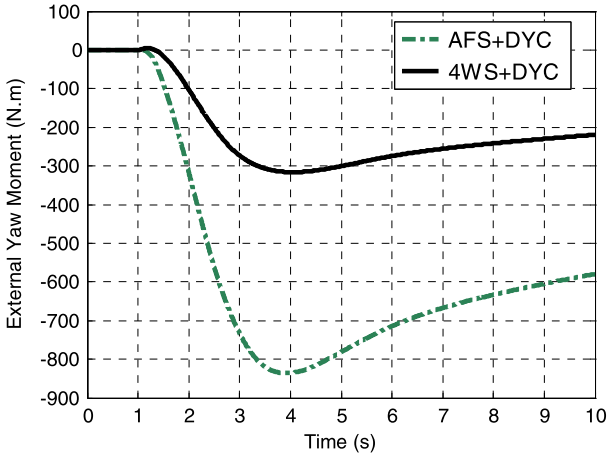

(e) External Yaw Moment

Since the steady-state value of $\dot{e}_1 = \dot{y}_e$ is zero, the steady-state value of vehicle side slip angle becomes

$$(\psi_e)_{ss} = -\beta_{ss}, \tag{32}$$

which shows that the steady-state error attains the magnitude of vehicle sideslip angle. Substituting Eq. (7) into Eq. (32) leads to

$$\beta_{ss} = -(\psi - \psi_d) \quad \Rightarrow \quad \beta_{ss} + \psi = \psi_d. \tag{33}$$

This means that the velocity vector is still in the same direction of the desired velocity.

4.2 Lane change maneuver

This maneuver is designed in such a way that the vehicle with a constant velocity of 30 m/s enters a lane change path of 120 m radius and then turns in an opposite path with the same radius and finishes on a straight line. The results are shown in Fig. 11.

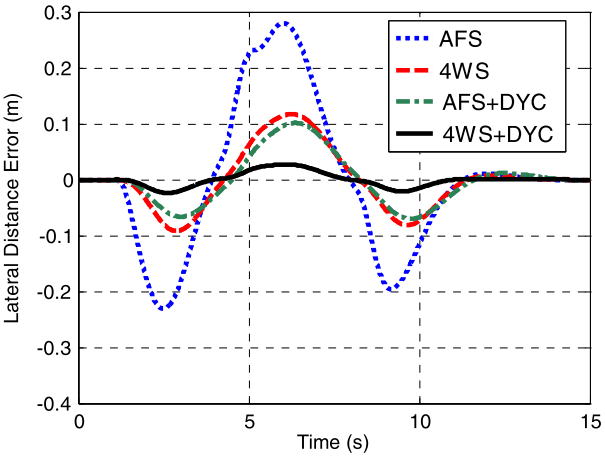

(a) Lateral distance error

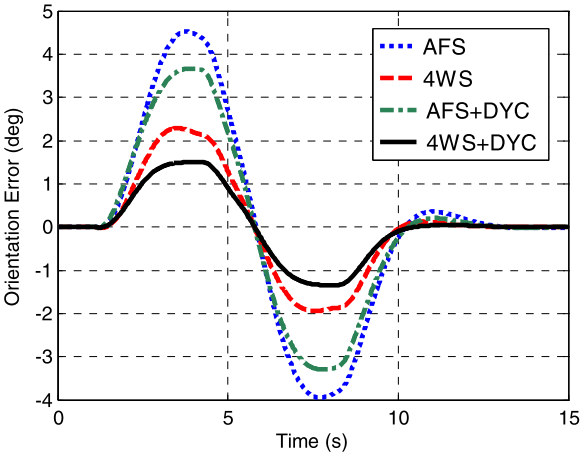

(b) Orientation error

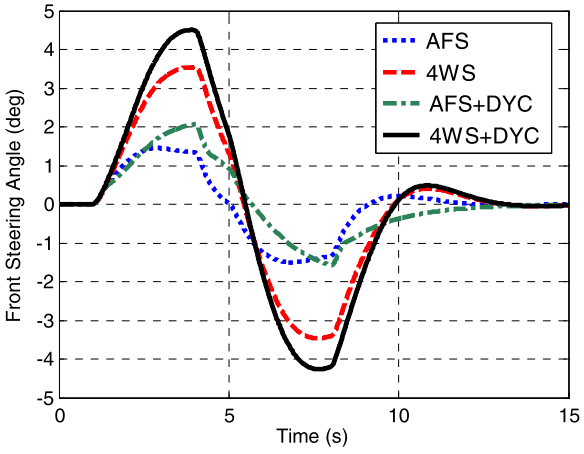

(c) Front steering angle

Fig. 11 Simulation results of the lane change maneuver

Fig. 11 (*Continued*)

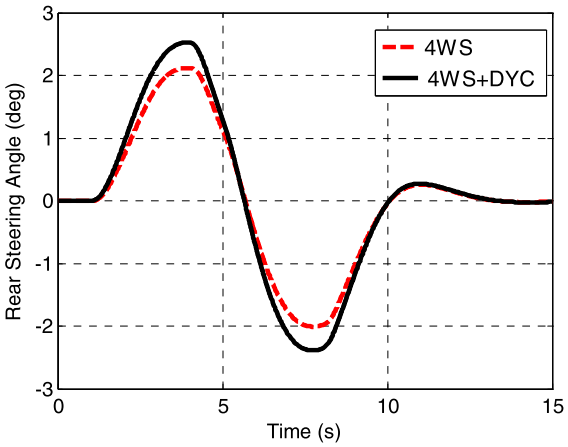

(d) Rear steering angle

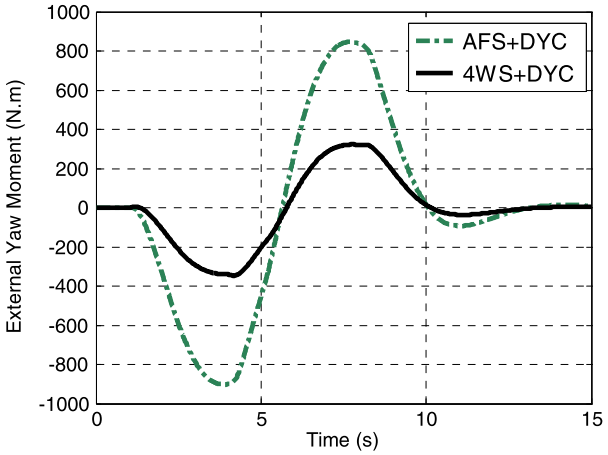

(e) External yaw moment

Again the values of both lateral and heading errors are considerably lower for the 4WS + DYC controller compared to those of the other controllers as shown in Figs. 11a and 11b. Once again, Figs. 11c and 11d show that the 4WS + DYC controller is able to use larger steer angles and properly adjust the force and moment resultants. Figure 11e illustrates the values of the corrective external yaw moment applied by the DYC system.

4.3 Robustness

During the vehicle motions, several parameters like mass, tire properties, and road friction may vary, and the robust controller must perform independently of the parameter variations. In this section the performance of the controllers on a low-friction road is investigated. The vehicle enters a circular pass of radius 120 m with a speed of 20 m/s on a road with a friction coefficient of 0.3. This is a severe maneuver in which the AFS controller is unable to hold the stability and the vehicle becomes out of control. The output results for the three other controllers are illustrated in Fig. 12. The results show that even the 4WS controller has an undesired fluctuating response and would become unstable if the speed (in fact lateral

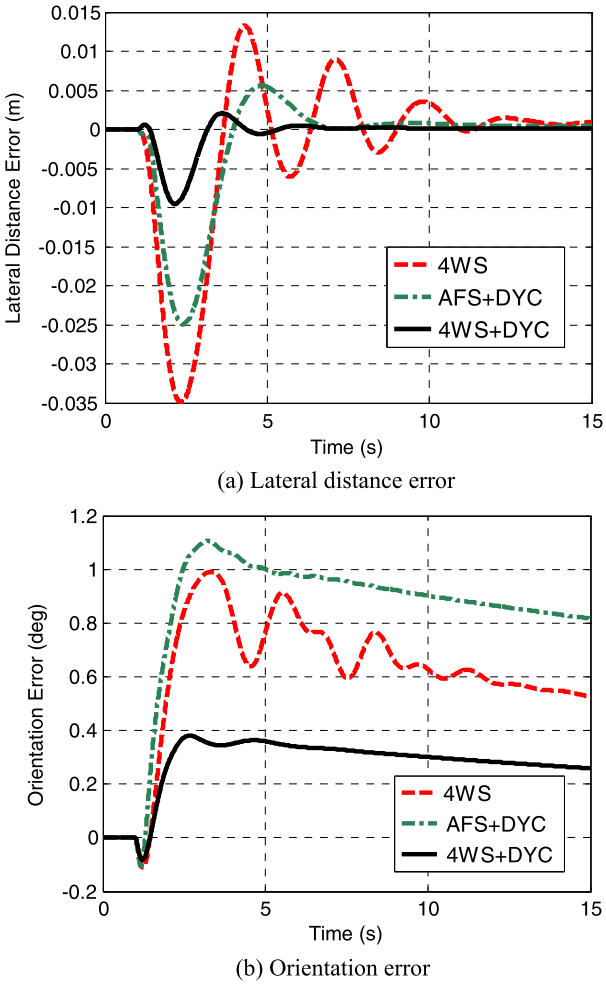

(a) Lateral distance error

(b) Orientation error

Fig. 12 Simulation results for a circular maneuver on the low-friction road

acceleration) was increased. The two other controllers incorporating the DYC, on the other hand, have more stable responses. The response of the 4WS + DYC controller is superior and is able to follow the pass with very low lateral and orientation errors.

4.4 Discussion

Unlike the AFS system, which only utilizes the front steering angle for controlling the desired path, the 4WS system in addition uses the rear steering angle and effectively reduces the vehicle yaw rate and side slip angle. The drawback of both AFS and 4WS systems is the limitation of tire lateral force at high lateral accelerations when the tire force levels off with increase of slip angle. The DYC system that uses the braking action has the advantage of working properly at high lateral accelerations. The addition of the DYC system to the controllers, therefore, is reasonable and was shown to be a suitable measure to improve the performance of the controllers. It was also effective in providing robustness against the parameter changes. It was observed that the combination of 4WS and DYC systems results in a

Table 3 Vehicle data

Parameter	Index	Value
Vehicle mass	m	1300 (kg)
Vehicle yaw moment of inertia	J	2500 (kg m^2)
Vehicle forward speed	u	30 (m/s)
Distance from front axle to c.g.	L_f	1.2 (m)
Distance from rear axle to c.g.	L_r	1.3 (m)
Front tire nominal cornering stiffness	$\bar{C}_{\alpha f}$	32000 (N/rad)
Rear tire nominal cornering stiffness	$\bar{C}_{\alpha r}$	32000 (N/rad)
Maximum perturbation on front tire cornering stiffness	Q_f	45 %
Maximum perturbation on rear tire cornering stiffness	Q_r	45 %

superior controller, which provides a good path following and stability as well as appropriate robustness against the parameter changes.

5 Conclusions

In this study the design of integrated controllers for automatic path following of vehicles was presented. The mathematical model was derived based on lateral and orientation errors that should be forced to vanish by the controller. Robust control theory using the μ-synthesis method was applied to design a controller that accounts for the uncertainties of vehicle model. Four types of control systems, namely AFS, 4WS, AFS + DYC, and 4WS + DYC were developed for comparison purposes. Numerical simulations were performed in order to assess the effectiveness of the controller and to compare the responses of the control types. Results provided for three different maneuvers, namely a circular path on a high friction road, a lane-change maneuver, and a low-friction circular path, indicated that not only the 4WS + DYC controller was able to follow the desired path with considerable low lateral and orientation errors, but also it had much better efficacy in comparison to the other controllers in all situations. This controller utilizes the maximum control potentials both in low and high lateral accelerations and when a parameter in vehicle motion is changed.

Appendix A

See Table 3.

Appendix B

Parametric relations and numerical values for matrices A_0, B_0, C_0, D_0, E_0, A_i, B_i, C_i, D_i, E_i, and G_{sys}.

$$A_0 = \begin{bmatrix} 0 & 1 & 0 & 0 \\ 0 & -2.4615 & 98.4615 & 0.1231 \\ 0 & 0 & 0 & 1 \\ 0 & 0.0640 & -2.56 & -2.0032 \end{bmatrix}, \qquad E_0 = \begin{bmatrix} 0 \\ -1595.1 \\ 0 \\ -80.1 \end{bmatrix},$$

$$B_0 = \begin{bmatrix} 0 & 0 & 0 \\ 49.2 & 49.2 & 0 \\ 0 & 0 & 0 \\ 30.7 & -33.3 & 0.0004 \end{bmatrix},$$

$$C_0 = \begin{bmatrix} 1 & 0 & 0 & 0 \\ 0 & 0 & 1 & 0 \end{bmatrix}, \qquad D_0^E = [0]_{2\times 1}, \qquad D_0^B = [0]_{2\times 3},$$

$$A_1 = \begin{bmatrix} 0 & 0 & 0 & 0 \\ 0 & -2\frac{C_{\alpha f} Q_f}{mu} & 2\frac{C_{\alpha f} Q_f}{m} & 2\frac{-C_{\alpha f} L_f Q_f}{mu} \\ 0 & 0 & 0 & 0 \\ 0 & 2\frac{-C_{\alpha f} L_f Q_f}{I_z u} & 2\frac{C_{\alpha f} L_f Q_f}{I_z} & -2\frac{C_{\alpha f} L_f^2 Q_f}{I_z u} \end{bmatrix}$$

$$= \begin{bmatrix} 0 & 0 & 0 & 0 \\ 0 & -0.5538 & 22.1538 & -0.6646 \\ 0 & 0 & 0 & 0 \\ 0 & -0.3456 & 13.8240 & -0.4147 \end{bmatrix},$$

$$B_1 = \begin{bmatrix} 0 & 0 & 0 \\ \frac{2C_{\alpha f} Q_f}{m} & 0 & 0 \\ 0 & 0 & 0 \\ \frac{2C_{\alpha f} L_f Q_f}{I_z} & 0 & 0 \end{bmatrix} = \begin{bmatrix} 0 & 0 & 0 \\ 22.1538 & 0 & 0 \\ 0 & 0 & 0 \\ 13.8240 & 0 & 0 \end{bmatrix},$$

$$E_1 = \begin{bmatrix} 0 \\ 2\frac{-C_{\alpha f} L_f Q_f}{m} \\ 0 \\ -2\frac{C_{\alpha f} L_f^2 Q_f}{I_z} \end{bmatrix} = \begin{bmatrix} 0 \\ -26.5846 \\ 0 \\ -16.5888 \end{bmatrix},$$

$$C_1 = [0]_{2\times 4}, \qquad D_1^E = [0]_{2\times 1}, \qquad D_1^B = [0]_{2\times 3},$$

$$A_2 = \begin{bmatrix} 0 & 0 & 0 & 0 \\ 0 & -2\frac{C_{\alpha r} Q_r}{mu} & 2\frac{C_{\alpha r} Q_r}{m} & 2\frac{C_{\alpha r} L_r Q_r}{mu} \\ 0 & 0 & 0 & 0 \\ 0 & 2\frac{C_{\alpha r} L_r Q_r}{I_z u} & 2\frac{-C_{\alpha r} L_r Q_r}{I_z} & -2\frac{C_{\alpha r} L_r^2 Q_r}{I_z u} \end{bmatrix}$$

$$= \begin{bmatrix} 0 & 0 & 0 & 0 \\ 0 & -0.5538 & 22.1538 & 0.72 \\ 0 & 0 & 0 & 0 \\ 0 & 0.3744 & -14.9760 & -0.4867 \end{bmatrix},$$

$$B_2 = \begin{bmatrix} 0 & 0 & 0 \\ 0 & \frac{2C_{\alpha r} Q_r}{m} & 0 \\ 0 & 0 & 0 \\ 0 & -\frac{2C_{\alpha r} L_r Q_r}{I_z} & 0 \end{bmatrix} = \begin{bmatrix} 0 & 0 & 0 \\ 0 & 22.1538 & 0 \\ 0 & 0 & 0 \\ 0 & -14.9760 & 0 \end{bmatrix},$$

$$E_2 = \begin{bmatrix} 0 \\ 2\frac{C_{\alpha r} L_r Q_r}{m} \\ 0 \\ -2\frac{C_{\alpha r} L_r^2 Q_r}{I_z} \end{bmatrix} = \begin{bmatrix} 0 \\ 28.8 \\ 0 \\ -19.4688 \end{bmatrix},$$

$$C_2 = [0]_{2\times 4}, \qquad D_2^E = [0]_{2\times 1}, \qquad D_2^B = [0]_{2\times 3},$$

$$G_{\text{sys}}(s) = \begin{bmatrix} 0 & 0.1 & 0 & 0 & 0 & 0 & 0 & 0 & 0 & 0 \\ 0 & -2.5 & 98.5 & 0.1 & 41.1 & 42.6 & -1595.1 & 49.2 & 49.2 & 0 \\ 0 & 0 & 0 & 1 & 0 & 0 & 0 & 0 & 0 & 0 \\ 0 & 0.1 & -2.6 & -2 & 25.6 & -28.8 & -80.1 & 30.7 & -33.3 & 0.0004 \\ 0 & -0.013 & 0.5 & -0.016 & 0 & 0 & -0.6 & 0.5 & 0 & 0 \\ 0 & -0.013 & 0.5 & 0.016 & 0 & 0 & 0.7 & 0 & 0.5 & 0 \\ 1 & 0 & 0 & 0 & 0 & 0 & 0 & 0 & 0 & 0 \\ 0 & 0 & 1 & 0 & 0 & 0 & 0 & 0 & 0 & 0 \end{bmatrix}.$$

References

1. El Hajjaji, A., Bentalba, S.: Fuzzy path tracking control for automatic steering of vehicles. Robot. Auton. Syst. **43**, 203–213 (2003)
2. Consolini, L., Piazzi, A., Tosques, M.: Path following of car-like vehicles using dynamic inversion. Int. J. Control **76**, 1724–1738 (2003)
3. Balluchi, A., Bicchi, A., Souères, P.: Path-following with abounded-curvature vehicle: a hybrid control approach. Int. J. Control **78**, 1228–1247 (2005)
4. Hellström, T., Ringdahl, O.: Follow the past: a path-tracking algorithm for autonomous vehicle. Int. J. Veh. Auton. Syst. **4**, 216–224 (2006)
5. Heredia, G., Ollero, A.: Stability of autonomous vehicle path tracking with pure delays in the control loop. Adv. Robot. **21**, 23–50 (2007)
6. Goodarzi, A., Sabooteh, A., Esamailzadeh, E.: Automatic path control based on integrated steering and external yaw-moment control. Proc. Inst. Mech. Eng., Proc., Part K, J. Multi-Body Dyn. **222**, 189–200 (2008)
7. Samar, R., Rehman, A.: Autonomous terrain-following for unmanned air vehicles. Mechatronics **21**(6), 844–860 (2010)
8. Feng, Z., Allen, R.: Reduced order H_∞ control of an autonomous underwater vehicle. Control Eng. Pract. **12**, 1511–1520 (2004)
9. Hiraoka, T., Nishihara, O., Kumamoto, H.: Automatic path-tracking controller of a four-wheel steering vehicle. Veh. Syst. Dyn. **47**, 1205–1227 (2009)
10. Moriwaki, K.: Autonomous steering control for electric vehicles using nonlinear state feedback H_∞ control. Nonlinear Anal. **63**, 2257–2268 (2005)
11. Ackermann, J., Guldner, J., Sienel, W., Steinhauser, R., Utkin, V.I.: Linear and nonlinear controller design for robust automatic steering. IEEE Trans. Control Syst. Technol. **3**, 132–143 (1998)
12. Ellis, J.R.: Vehicle Handling Dynamics. Mechanical Engineering Publications, London (1994)
13. Rajamani, R.: Vehicle Dynamics and Control. Springer, Berlin (2006)
14. Zhou, K., Doyle, J.C.: Essentials of Robust Control. Prentice Hall, New York (1999)
15. Doyle, J.C.: Structured uncertainty in control system design. In: Proceedings of the 24 IEEE Conference on Decision and Control, pp. 260–265 (1985)
16. Mashadi, B., Majidi, M.: Integrated AFS/DYC sliding mode controller for a hybrid electric vehicle. Int. J. Veh. Des. **56**(1/2/3/4), 246–269 (2011)
17. Mathworks: Documentation and help. MATLAB© 7.9 (2009)
18. Pacejka, H.B.: Tyre and Vehicle Dynamics. Elsevier/Butterworth-Heinemann, Amsterdam/Oxford (2002)